Altering gain of the infralimbic-to-accumbens shell circuit alters economically dissociable decision-making algorithms

Brian M. Sweis[a,b,c], Erin B. Larson[c], A. David Redish[c,1], and Mark J. Thomas[c,d]

[a]Graduate Program in Neuroscience, University of Minnesota, Minneapolis, MN 55455; [b]Medical Scientist Training Program, University of Minnesota, Minneapolis, MN 55455; [c]Department of Neuroscience, University of Minnesota, Minneapolis, MN 55455; and [d]Department of Psychology, University of Minnesota, Minneapolis, MN 55455

Edited by Robert Malenka, Stanford University School of Medicine, Stanford, CA, and approved May 21, 2018 (received for review February 20, 2018)

The nucleus accumbens shell (NAcSh) is involved in reward valuation. Excitatory projections from infralimbic cortex (IL) to NAcSh undergo synaptic remodeling in rodent models of addiction and enable the extinction of disadvantageous behaviors. However, how the strength of synaptic transmission of the IL–NAcSh circuit affects decision-making information processing and reward valuation remains unknown, particularly because these processes can conflict within a given trial and particularly given recent data suggesting that decisions arise from separable information-processing algorithms. The approach of many neuromodulation studies is to disrupt information flow during on-going behaviors; however, this limits the interpretation of endogenous encoding of computational processes. Furthermore, many studies are limited by the use of simple behavioral tests of value which are unable to dissociate neurally distinct decision-making algorithms. We optogenetically altered the strength of synaptic transmission between glutamatergic IL–NAcSh projections in mice trained on a neuroeconomic task capable of separating multiple valuation processes. We found that induction of long-term depression in these synapses produced lasting changes in foraging processes without disrupting deliberative processes. Mice displayed inflated reevaluations to stay when deciding whether to abandon continued reward-seeking investments but displayed no changes during initial commitment decisions. We also developed an ensemble-level measure of circuit-specific plasticity that revealed individual differences in foraging valuation tendencies. Our results demonstrate that alterations in projection-specific synaptic strength between the IL and the NAcSh are capable of augmenting self-control economic valuations within a particular decision-making modality and suggest that the valuation mechanisms for these multiple decision-making modalities arise from different circuits.

neuroeconomics | mice | optogenetics | plasticity | decision-making

Addiction, like many other neuropsychiatric disorders, is often characterized by an inability to regulate maladaptive motivated behaviors, particularly after continued drug use (1). Recent advances in neuroscience have begun to dissect reward-related circuitry to understand how specific circuits change over time during addiction (2, 3). Targeting such disorders with plasticity-altering manipulations could prove extremely useful to provide long-lasting treatments that can modify disease trajectory and prevent recovering addicts from making poor decisions that lead to relapse.

There is an intimate link between memory and decision-making (4). Weights of synaptic inputs change as a consequence of learning and carry information, including experiences related to addiction (5, 6). How information is stored changes how it is processed during decision-making (4). However, how the synaptic efficacy of a specific circuit impacts distinct aspects of decision-making information processing has been largely unexplored. Only recently have tools been developed to directly manipulate the plasticity of specific inputs. Thus, direct interrogation of the synaptic efficacy of specific circuits is critical for our understanding of decision-making information processing and disease etiology. Such approaches will be critical for the development of lasting disease-augmenting neuromodulation therapies.

The shell of the nucleus accumbens (NAcSh) is a specialized region of the striatum where reward valuations are encoded and where motivation is thought to be translated into reward-seeking actions (7–9). The NAcSh receives dense, direct excitatory input projections from the infralimbic (IL) cortex, a subregion of the prefrontal cortex that has been implicated in the learning and maintenance of cognitive flexibility and self-control (10). Thus, the IL–NAcSh circuit is in a key position to serve as a critical conduit mediating information flow that integrates regulatory higher-order cognitive processes with reward-seeking motivated behavioral output processes (10).

The IL–NAcSh circuit is highly susceptible to the effects of drug-related experiences. In humans, functional connectivity of an analogous circuit is augmented in recovering drug users (11). fMRI studies that followed abstinent drug users found that the strength of functional connectivity [coherence in resting-state blood oxygenation level-dependent (BOLD) signal] between the medial prefrontal cortex and nucleus accumbens was weaker in individuals who relapsed sooner, consistent with an hypothesized

Significance

Synaptic remodeling in the infralimbic-to-accumbens shell (IL–NAcSh) circuit is linked to addiction relapse susceptibility; however, how these changes interact with decision-making computations remains unclear. We develop a neurophysiological assay to measure the strength of a specific circuit at the ensemble level. We then use that assay in combination with a neuroeconomic task to provide causal evidence that synaptic strength of the IL–NAcSh mediates distinct aspects of decision-making information processing. We find that individual differences in IL–NAcSh strength mediate reevaluations behaviorally resolvable from parallel, co-occurring deliberative valuations. An important implication of our work is that acutely delivered circuit-specific plasticity manipulations can produce long-lasting computation-specific effects on certain kinds of choices and can potentially serve as a therapeutic neuromodulation intervention.

Author contributions: B.M.S., A.D.R., and M.J.T. designed research; B.M.S., E.B.L., A.D.R., and M.J.T. performed research; B.M.S., A.D.R., and M.J.T. contributed new reagents/analytic tools; B.M.S., A.D.R., and M.J.T. analyzed data; and B.M.S., A.D.R., and M.J.T. wrote the paper.

The authors declare no conflict of interest.

This article is a PNAS Direct Submission.

[1]To whom correspondence should be addressed. Email: redish@umn.edu.

This article contains supporting information online at www.pnas.org/lookup/suppl/doi:10.1073/pnas.1803084115/-/DCSupplemental.

prefrontal role in overriding accumbens-driven relapse behaviors (11). In parallel, several animal models of addiction produce plasticity in the synaptic efficacy in the IL–NAcSh circuit, particularly at times of decision-making vulnerabilities that often lead to drug relapse (12–16). These data suggest that a key factor in addiction lies in experience-dependent circuit plasticity across this circuit, both over the course of abstinence from drugs of abuse as individuals transition into long-lasting decision-vulnerable states as well as immediately following an acute trigger of relapse. Thus, it is clear that the IL–NAcSh circuit has an important role in addiction etiology. However, current theories of decision-making suggest that decision arises from multiple separable decision-making systems, and current theories of addiction suggest that addiction can arise from multiple failure points within those decision-making systems (17–21). How the IL–NAcSh circuit interacts with different decision points remains unknown.

Current approaches in systems neuroscience have not directly interrogated the functional consequences of circuit-specific synaptic remodeling on decision-making information processing. Instead, the majority of recent neuromodulation studies manipulate brain activity during on-going behaviors. Direct optogenetic inhibition of the IL–NAcSh pathway can cause spontaneous reinstatement or enhance cue-induced reinstatement of extinguished reward-seeking behaviors, while excitation of the IL–NAcSh pathway during cue presentation can block reinstatement of extinguished reward-seeking behaviors (10, 22–26). Such studies can easily probe the necessity for and sufficiency of the IL-NAcSh circuit in discrete regulatory processes with temporal precision. However, such "on-line" manipulations during on-going behaviors in real time impose disruptions of endogenous neural signaling and provide little insight into the functional consequences of synaptic remodeling on behavior.

An alternative approach is to alter the synaptic efficacy of signal transmission specifically of the IL–NAcSh circuit through optogenetically driven alterations in synaptic plasticity. Importantly, the goal of this approach is to change the gain of the information endogenously transmitted through this circuit, not to disrupt the information itself that is coded in this specific circuit. Thus, these types of manipulations should be delivered "off-line," outside of behavioral testing. Such an approach leaves endogenous information processing intact during behavioral observations measured at a later time point, when the functional consequences of lasting changes in circuit gain are realized. To date, only a handful of studies have directly augmented the strength of synaptic transmission of glutamatergic IL afferents in the NAcSh (13–15, 27). However, these studies have revealed conflicting findings, suppressing reward-seeking reinstatement in some cases but precipitating reinstatement in others.

Importantly, these studies have relied on relatively simple behavioral tests of value and compulsive drug-seeking behavior. Recent theories in neuroeconomics suggest that decisions made in different situations derive from different valuation functions residing in separable neural circuits (17, 20). It can be difficult to behaviorally segregate these parallel information-processing algorithms using traditional behavioral tasks (28). Neurally distinct computations can produce what (superficially) appear to be similar behaviors. Unless a task is specifically designed to separate them, behavioral consequences of distinct neural computations can appear grossly similar and thus remain inseparable. To discriminate neural computations through behavior and thus reveal circuit-specific information processing, we applied off-line plasticity manipulations of the IL–NAcSh circuit in mice that learned a complex neuroeconomic task which is capable of separating behavioral consequences among different decision-making systems.

Here, we combine these two approaches: circuit-specific off-line manipulations of the strength of IL–NAcSh synaptic transmission with complex behavioral testing designed to dissociate existing neuroeconomic theories of parallel valuation systems. We adopted a neuroeconomic task, Restaurant Row, for use in mice that separates deliberative valuation algorithms from foraging valuation algorithms for natural rewards within the same trial (29, 30). We observed changes in separable aspects of behavior in foraging valuations but not deliberative valuations that may more closely reflect changes in dissociable neural computations that underlie those dissociable behaviors. In doing so, we also discovered and developed a straightforward way to measure individual differences in the projection-specific strength of synaptic transmission at the neuronal population ensemble level.

Results

Projection-Specific Targeting of the IL–NAcSh Circuit. To gain input-specific control of the IL–NAcSh circuit, we bilaterally transfected IL neurons in male mice via intracranial infusions of an adeno-associated viral (AAV8) construct containing the gene for Chronos (31), a light-gated fast-kinetics cation-channel opsin, fused to a GFP reporter driven by the neuron-specific synapsin (Syn) promoter (Fig. 1*A* and *SI Appendix*, Fig. S1). This promoter directed Chronos expression specifically to neurons, projections of which out of the IL are largely comprised of excitatory, pyramidal glutamatergic efferent axons. Then, we bilaterally implanted mice with optic fiber ferrules directed at the NAcSh intended to illuminate and activate Chronos-containing axon terminals originating from the IL with blue light in vivo. Furthermore, IL projections to the ventral striatum preferentially innervate the NAcSh while nearby cortical regions such as the prelimbic cortex preferentially innervate the nucleus accumbens core (32, 33). This difference in anatomical topographical organization helped ensure that unintentional virus transfection outside the IL was less likely to cross-contaminate the manipulation of the target IL–NAcSh circuit. We then allowed mice to recover to allow robust expression and anterograde transport of Chronos downstream along IL axons delivering opsins to IL terminals in NAcSh.

Pharmacological Characterization of Pre- and Postsynaptic Components of Optogenetically Evoked IL–NAcSh Field Potentials. To test the effect of our IL–NAcSh circuit manipulation, we directly recorded the electrophysiology of the IL–NAcSh circuit from parasagittal brain slices that contained the NAcSh and preserved functional IL axon projections (Fig. 1*B* and *SI Appendix*, Fig. S2). We performed these experiments in slices ex vivo to ensure we were directly recording in the NAcSh and could visualize dense IL afferent fiber bundles. This approach also allowed us to test concurrent, serial pharmacological assays that together characterize the waveform of optogenetically evoked field potentials in this circuit not previously demonstrated. By placing an extracellular recording electrode directly in the NAcSh and illuminating a focal area of the surrounding tissue with blue light, we recorded light-evoked population potentials of the IL–NAcSh circuit. This reliably evoked a population potential with a waveform consisting of two negative peaks, labeled "N1" and "N2" (Fig. 1*B* and *SI Appendix*, Fig. S3). We found that only the N2 component required extracellular calcium (one-sample t tests normalized to baseline compared with 1.0; N1: zero calcium, $t = -0.01$, $P = 0.99$, calcium wash-in: $t = 0.03$, $P = 0.98$; N2: zero calcium, $t = -22.4$, $P < 0.0001$, calcium wash-in, $t = -1.5$, $P = 0.19$) and was blocked by the AMPA receptor (AMPR) antagonist DNQX in a dose-dependent manner (N1: 1 μM, $t = 1.1$, $P = 0.33$, 10 μM, $t = -0.7$, $P = 0.50$; N2: 1 μM, $t = -29.6$, $P < 0.0001$, 10 μM, $t = -58.1$, $P < 0.0001$, 1 μM vs. 10 μM, $t = -10.9$, $P < 0.0001$), suggesting that glutamate release from synaptic vesicles within IL terminals in response to light drove the N2 component of the waveform, which reflected the excitatory postsynaptic (NAcSh) population potential of the IL–NAcSh circuit (Fig. 1*B* and *SI Appendix*,

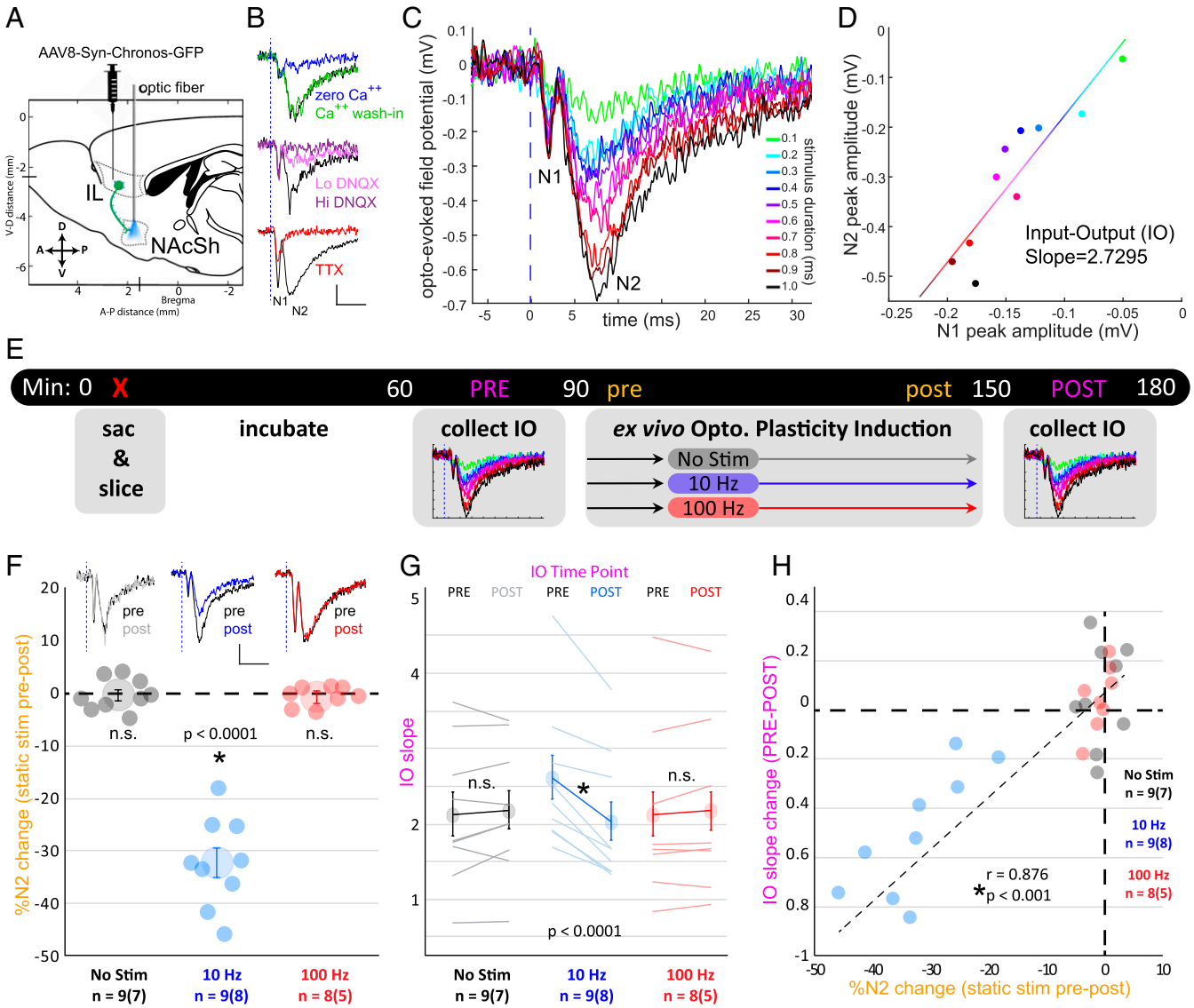

Fig. 1. Optogenetically driven induction of plasticity in the IL–NAcSh circuit augments an ensemble-level metric of synaptic strength. (*A*) Surgical schematic, parasagittal view. Mice were bilaterally transfected in the IL with an AAV8 construct containing the gene for Chronos driven by a Syn promoter with a fusion GFP reporter. (*B*) Pharmacological characterization of bimodal light-evoked field potentials recorded ex vivo in the NAcSh. The vertical dashed blue line indicates a 1-ms light pulse. (*Top*) The zero-calcium bath reversibly abolished the N2 component. (*Middle*) The AMPAR antagonist abolished the N2 component dose dependently. (*Bottom*) TTX abolished the N2 component, reducing the N1 component. (Scale bars: *x* axis, 10 ms; *y* axis, 0.2 mV.) (*C*) An example of the IO regimen assayed on a single slice. Stimulus duration was varied from 0.1 to 1.0 ms. (*D*) N1 and N2 peak amplitudes are plotted from examples of traces in *C*, and the linear regression slope was calculated. To test if the IO slope can serve as an independent metric of circuit-specific synaptic strength, IO ramps were assayed before and after ex vivo bath application of plasticity-inducing optogenetic stimulation protocols. (*E*) Experimental timeline. Mice were killed and slices were prepared at time 0. After allowing 1 h for tissue incubation, the first IO slope (pink PRE in timeline) was collected. From this, the stimulus duration that elicited 50% of the maximum N2 amplitude was determined and was used as the static stimulus parameter during regular samplings for the bath-application plasticity assay [12.5 min baseline sampling (gold pre in timeline), followed by one of three protocols and then 37.5 min of additional sampling; the final 12.5 min served as the gold post in timeline]. A second postplasticity IO slope assay was collected (pink POST in timeline). (*F*) The percent of N2 change normalized to baseline sampling (gold pre and post time points in timeline). Representative waveform traces were plotted from gold pre and post time points in timeline for each protocol. (Scale bars: *x* axis, 10 ms; *y* axis, 0.2 mV.) (*G*) IO slopes from pink PRE and POST time points in timeline. (*H*) The percentage of N2 change in *F* plotted against the change in IO slope in *G*, with Pearson correlation, *r*. Dots in *F* and *H* and thin lines in *G* represent individual slices. Sample size in *F* and *G* is noted below the *x* axis as the number of slices followed by number of mice in parentheses. Larger dots represent mean ± 1 SE. **P* = value shown on plot; n.s., not significant.

Fig. S3). This suggested that the earlier N1 component reflected evoked presynaptic firing activity in collective IL axons terminating in the NAcSh. We found that application of 1 μM of the voltage-gated sodium channel antagonist TTX abolished the N2 peak ($t = -111.8$, $P < 0.0001$) and, surprisingly, did not abolish the N1 peak but instead reduced it (<1, $t = -10.6$, $P < 0.0001$; >0, $t = 10.5$, $P < 0.0001$) (Fig. 1*B* and *SI Appendix*, Fig. S3). This suggests that while IL axons were not capable of eliciting action potentials in the presence of TTX, direct opsin activity was still detectable in IL population fibers but was insufficient to drive terminal synaptic release of glutamate. The timing of such events indicates this bimodal waveform is monosynaptic.

Assaying Optogenetically Driven Induction of Plasticity in IL–NAcSh Optogenetically Evoked Field Potentials. To determine the extent to which these measurements are sensitive to the induction of

long-term plasticity in the IL–NAcSh circuit, we recorded light-evoked population responses from slice preparations before and after applying a stimulation protocol previously shown to induce changes in plasticity in the nucleus accumbens (Fig. 1 *E* and *F* and *SI Appendix*, Fig. S4) (13–15, 34). Prolonged 10-Hz stimulation (10 min, 4-ms pulses) caused a sustained reduction in the peak amplitude of the N2 component of the light-evoked population response (one-sample *t* tests normalized to baseline compared with 1.0, $t = -6.7$, $P < 0.0001$) while having no lasting effect on the N1 component ($t = 0.9$, $P = 0.36$) (*SI Appendix*, Fig. S4). Consistent with past reports, this suggests that the 10-Hz protocol can induce long-term depression (LTD) in the IL–NAcSh circuit, decreasing NAcSh responsivity to IL recruitment (13–15, 34). We tested this against a different stimulation protocol. We found no changes in either the N1 or N2 components following 100-Hz burst stimulations (1-s train, 4-ms pulses, four trains, 10-s intertrain interval: N1: $t = 1.6$, $P = 0.18$; N2: $t = 0.7$, $P = 0.53$) (Fig. 1*F* and *SI Appendix*, Fig. S4). This appeared no different from slices that received neither 10-Hz nor 100-Hz stimulation (N1: $t = 0.4$, $P = 0.69$; N2: $t = 0.7$, $P = 0.51$) (Fig. 1*F* and *SI Appendix*, Fig. S4).

Optogenetic Measurement of the Functional Strength of the IL–NAcSh Circuit at the Ensemble Level. Measuring the strength of synaptic transmission of a specific neural pathway that can be compared across subjects has many challenges. Between-subject differences that can alter extracellular voltage readings include the virus transfection rate, opsin expression level, slice preparation cut angle, tissue health, density of IL nerve terminals or NAcSh cell bodies, and the placement of the recording electrode, among others. One means of circumventing these issues in comparing the degree of synaptic strength across subjects is to measure evoked AMPAR/NMDA receptor (NMDAR) current ratios with whole-cell patch-clamp recordings (35). Thus, while optogenetically evoked AMPAR/NMDAR ratios can also provide input-specific readings of the strength of synaptic transmissions, these measures reflect activity at only the single-cell level (13). Here, the clear distinction between the presynaptic and postsynaptic components of the IL–NAcSh circuit in this light-evoked population waveform provides a possibility to normalize the size of the NAcSh response (N2) to the degree of IL recruitment (N1). Although the relative sizes of N1 and N2 can change due to the aforementioned issues (e.g., electrode placement), the relative changes between N1 and N2 in response to alterations in stimulation drive should provide an accurate measure of the strength of synaptic transmission in this circuit. We tested the input–output (IO) relationship in NAcSh brain slices from mice in different treatment groups by ramping up and ramping down the stimulus drive (here, the stimulus duration) and measuring peak N1 and N2 amplitudes (Fig. 1 *C* and *D*). The slope of the resulting curve yields a metric of the functional synaptic strength of the IL–NAcSh circuit that should be comparable across animals (Fig. 1*D*).

Optogenetically Induced Plasticity in the IL–NAcSh Circuit Is Detected by an Ensemble-Level Metric of Synaptic Strength. To validate the light-evoked IO relationship as a metric of the strength of synaptic transmission in the IL–NAcSh circuit recorded at the population level, we applied the IO assay in slice preparations before and after applying plasticity protocols (no, 10-Hz, or 100-Hz stimulation) (Fig. 1 *E* and *G*). In each slice, we determined the stimulation value that elicited a 50% half-maximum response in the initial IO assay (mean stimulation duration used for static tests: 0.678 ± 0.045 ms) and used this value as the test stimulus during the readings before and after the plasticity induction protocol (the stimulation used during application of the 10-Hz and 100-Hz protocols was always 4-ms pulses). The final IO assay always used the same stimulation regimen as the initial IO assay. We found that only the 10-Hz protocol caused a significant decrease in the IO relationship between N1 and N2 response pairs when comparing the final IO assay with the initial IO assay (paired *t* test, no stimulation: $t = 0.8$, $P = 0.43$; 10 Hz: $t = -5.3$, $P < 0.0001$; 100 Hz: $t = 1.0$, $P = 0.36$) (Fig. 1*G* and *SI Appendix*, Fig. S5). That is, upon additional recruitment of IL activity, less proportional recruitment of NAcSh responsivity was measured following an LTD-inducing stimulation protocol. Furthermore, the degree of change in the IO relationship was significantly correlated with the degree of peak N2 amplitude change in static readings following plasticity induction relative to baseline static readings (Pearson $r = 0.876$, $P < 0.001$) (Fig. 1*H*; see Fig. 1*F* and *SI Appendix*, Fig. S4 for the percent of N2 change during static stimulations). Thus, the IO relationship provides a useful means of measuring the strength of synaptic transmission in the IL–NAcSh circuit that is sensitive to a plasticity-inducing stimulation protocol and can be measured at the population level.

Optogenetic Measurement of IL–NAcSh Synaptic Strength Captures in Vivo Manipulations of Plasticity Comparable Across Subjects. To test if this IO assay could capture changes in synaptic strength in response to a plasticity-inducing protocol delivered in vivo that was comparable between animals, we delivered no-stimulation, 10-Hz, or 100-Hz protocols to mice implanted with optic fibers directed at the NAcSh 24 h before mice were killed and ex vivo recording was performed (Fig. 2*A*). Use of the IO assay revealed that only the 10-Hz protocol group had a significantly reduced IO relationship metric, reflecting successful in vivo induction of LTD of the IL–NAcSh circuit (one-way ANOVA, $F = 8.0$, $P < 0.01$, post hoc Tukey comparisons: no stimulation vs. 10 Hz: $t = 3.3$, $P < 0.01$; no stimulation vs. 100 Hz: $t = -0.5$, $P = 0.88$; 10 Hz vs. 100 Hz: $t = -3.7$, $P < 0.01$) (Fig. 2*B*). This confirms that an absolute metric of the comparable strength of IL–NAcSh synaptic transmission between subjects can be measured at the

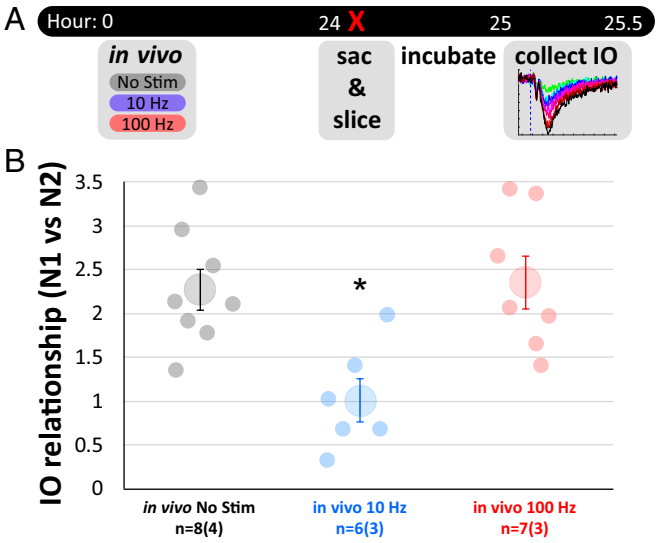

Fig. 2. The optogenetic IO slope collected ex vivo captures a between-subjects measure of IL–NAcSh synaptic strength sensitive to in vivo manipulations of plasticity. (*A*) Experimental timeline. Mice were given no-stimulation, 10-Hz, or 100-Hz protocols in vivo at time 0. After 24 h, mice were killed, and slices were prepared. Following slice incubation recovery, the IO regimen was assayed to compare group differences in the strength of IL–NAcSh synaptic transmission. (*B*) Only mice receiving the 10-Hz protocol showed a significant decrease in IO slopes measured in the N1 vs. N2 relationship in the IO assay. Dots represent individual slices. Sample size is noted below the *x* axis as the number of slices followed by the number of mice in parentheses. Larger dots represent the mean ± 1 SE. *$P < 0.01$.

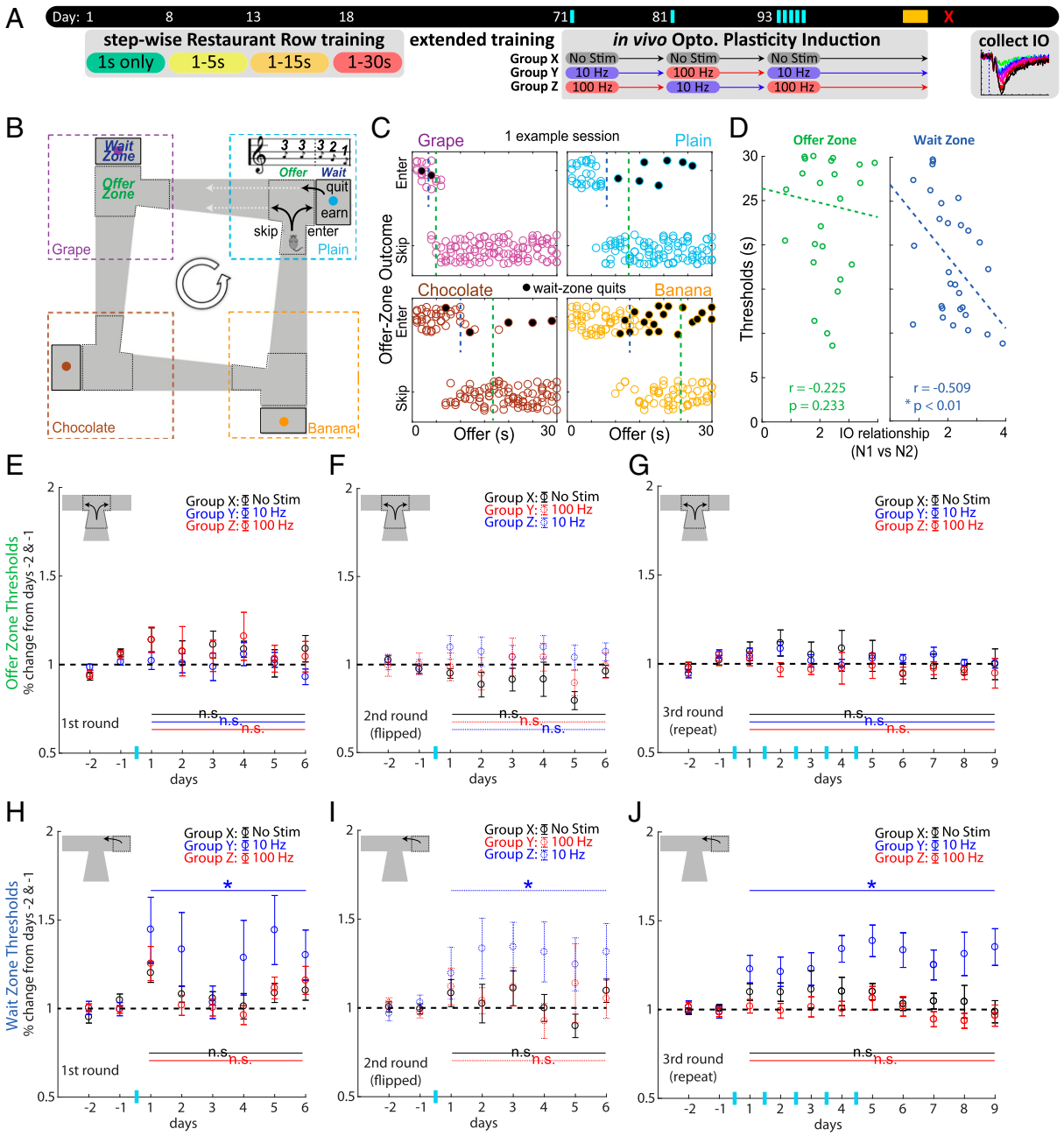

Fig. 3. Individual differences in the synaptic strength of the IL–NAcSh circuit are causally linked to distinct aspects of neuroeconomic decision-making valuations. (*A*) Experimental timeline. Thirty mice went through 70 consecutive days of testing in the Restaurant Row task. After day 18, mice were exposed to a number of offers ranging from 1 s to 30 s for the remainder of the experiment. Mice were then divided into three groups (X, Y, and Z, $n = 10$ each). On the evening of day 71, outside testing hours, mice received the no-stimulation, 10-Hz, or 100-Hz protocol (round 1) and then resumed normal daily Restaurant Row testing. On the evening of day 81 mice received round 2 of the stimulation protocols, with the assignments of groups Y and Z flipped in a repeated-measures cross-over design. After day 93, mice received round 3 of stimulation protocols under the original group assignments for five consecutive evenings. Following behavioral testing, all mice were killed for synaptic strength IO assays. (*B*) Schematic of the Restaurant Row task. Food-restricted mice were trained on a maze encountering serial offers for flavored rewards in four restaurants. Restaurant flavor and location were fixed and signaled via contextual cues. Each restaurant contained a separate offer zone and a wait zone. Tones sounded in the offer zone; a fixed tone pitch indicated a delay (1–30 s, randomly selected); to obtain food, mice would have to wait in the wait zone for the indicated delay duration. The tone pitch descended in the wait zone during the delay countdown. Mice could quit the wait zone for the next restaurant during the countdown, terminating the trial. Mice were tested daily for 60 min, earning their only source of food for the day. (*C*) An example of a session with individual trials plotted as dots: Mice entered low-delay restaurants and skipped high-delay restaurants in the offer zone, while sometimes quitting once in the wait zone (black dots). Dashed vertical lines represent calculated offer-zone (green) and wait-zone (blue) thresholds of willingness to budget time. Thresholds were measured from the inflection point of fitting a sigmoid curve to enters vs. skips or earns vs. quits as a function of delay cost. (*D*) Only wait-zone thresholds correlated significantly (negatively) with the synaptic strength of IL–NAcSh; offer-zone thresholds did not. Dots represent individual mice. Behavior was taken from final 5 d of testing (gold indicator on timeline in *A*). (*E–J*) Only wait-zone (*H–J*) and not offer-zone (*E–G*) thresholds changed significantly (increased) following the 10-Hz protocol delivery relative to days preceding stimulation in rounds 1 (*E* and *H*), 2 (*F* and *I*), and 3 (*G* and *J*). Plotted dots represent group means across mice ± 1 SE. *$P < 0.0001$ unless otherwise noted; n.s., not significant.

neuronal population level and that the 10-Hz manipulation decreases synaptic strength in vivo.

Individual Differences in the Synaptic Strength of the IL–NAcSh Circuit Are Causally Linked to Distinct Aspects of Neuroeconomic Decision-Making Valuations. To test the role of the strength of synaptic transmission in the IL–NAcSh circuit in complex valuation processes, following virus transfection of IL and optic fiber implantation in NAcSh, a separate cohort of mice was trained on a variant of a neuroeconomic decision-making task [Restaurant Row (29, 30)] to work for food in a self-paced manner. In this task, food-restricted mice had 1 h to work for their sole source of food for the day. Thus, this was an economic task in which time must be budgeted to become self-sufficient across days.

Mice traversed a square maze with four feeding sites (restaurants), each with unique spatial cues and each providing a different flavor (Fig. 3*B*). On entry into each restaurant, mice were informed of the delay that they would experience before getting the food from that restaurant. Mice could then either stay (waiting out the delay) or skip (proceeding on to the next restaurant). Mice revealed preferences for different flavors that varied among animals but were stable across days, indicating subjective valuations for each flavor were used to guide motivated behaviors. Varying the flavors, as opposed to varying the pellet number, allowed us to manipulate reward value without introducing differences in feeding times (as time is a limited commodity) between restaurants. Flavor preferences were stable across days (*SI Appendix*, Fig. S6). Costs were measured as the different delays mice would have to wait to earn a food reward on that trial, detracting from their session's limited 1-h time budget. Delays were randomly selected from offers ranging from 1 s to 30 s. Tones sounded upon restaurant entry, with pitch indicating offer cost. Mice learned to deliberate upon offer onset and discriminate between costs based on cued tones, typically rejecting high-cost offers and accepting low-cost offers (*SI Appendix*, Fig. S7). Taken together, in this task mice must make serial judgements in a self-paced manner weighing subjective valuations for different flavors against offer costs, balancing the economic utility of sustaining overall food intake against earning more rewards of a desirable flavor. In doing so, cognitive flexibility and self-control become critical components of the decision-making valuation processes in this task.

Furthermore, each restaurant contained two distinct zones: an offer zone and a wait zone. Mice were informed of the delay on entry into the offer zone, but delay countdowns did not begin until mice moved into the wait zone. After making an initial enter decision, mice had the opportunity to make a secondary, reevaluative decision to abandon the wait zone (quit) during delay countdowns. Mice were trained in stepwise stages of increasing ranges of offer costs (Fig. 3*A*) that initially trained mice to accept the majority of offers in the offer zone when all costs were relatively inexpensive, and they subsequently learned to quit as costs increased in the later stages of training (*SI Appendix, Supplementary Materials and Methods*).

To capture economic valuations of two different stages of decision-making information processing, we calculated separate offer-zone thresholds of willingness to enter and wait-zone thresholds of willingness to wait. Sigmoid curves were fit to enter/skip decisions or earn/quit decisions as a function of offer delay, and inflection points of each curve were calculated for offer-zone and wait-zone thresholds, respectively (Fig. 3*C*).

On completing their behavioral training, we separated mice into three experimental groups that determined which stimulation protocols they would each receive (Fig. 3*A*). As noted above, only the 10-Hz stimulation protocol alters the synaptic strength of the IL–NAcSh circuit. All stimulation protocols took place in the evening 4 h after mice completed testing in Restaurant Row for that day. We also divided the experimental timeline into three rounds of stimulation exposure and varied the protocol sequence order and repetition number to allow between-group as well as within-group comparisons. For the first round of stimulation exposure (Fig. 3*A*, first cyan time point), mice received one evening of their assigned stimulation protocol and were tested as usual in Restaurant Row for the next 10 d. After this 10th day of Restaurant Row testing, for the second round of stimulation exposure (Fig. 3*A*, second cyan time point), mice received one evening of the opposite stimulation protocol and were tested for an additional 10 d in Restaurant Row. Last, for the third round of stimulation exposure (Fig. 3*A*, cyan time point train), mice received five consecutive evenings of their original stimulation protocol assignments and were tested in Restaurant Row for the remaining days of the experiment.

We normalized offer-zone and wait-zone thresholds to 2 d of stable testing before each round of stimulation exposure and measured any changes in thresholds relative to baseline over the subsequent days. We found that across all days of testing, regardless of time point, no changes were observed in offer-zone thresholds in any experimental group (repeated-measures two-way mixed ANOVA comparing stimulation condition × day with mouse as a random variable; round 1: $F = 0.67$, $P = 0.51$; round 2: $F = 2.46$, $P = 0.11$; round 3: $F = 0.68$, $P = 0.51$) (Fig. 3 *E–G*). However, we found significant increases in wait-zone thresholds in the animals receiving the 10-Hz stimulation protocol in each of the three rounds of simulation exposure (Fig. 3 *H–J* and *SI Appendix*, Table S1). This effect was most robust in the third round of stimulation exposure with repeated evenings of stimulation and persisted for several days after the final protocol exposure (Fig. 3*J*). Mice displayed no changes in number of laps run, food intake, or locomotion (repeated-measures two-way mixed ANOVA comparing stimulation condition × time point with mouse as a random variable, laps: $F = 1.42$, $P = 0.26$; pellets earned: $F = 0.54$, $P = 0.59$; travel time between restaurants: $F = 1.23$, $P = 0.31$) (*SI Appendix*, Fig. S8). No gross changes in task learning were observed (*SI Appendix*, Fig. S9). Changes in behavior were specific to valuations made in the wait zone and not the offer zone, with reductions in quit decisions but no change in enter/skip decisions in the 10-Hz group (*SI Appendix*, Figs. S10 and S11). Furthermore, LTD of the IL–NAcSh circuit disrupted not only the frequency of quit events but also the economic characteristics of quit decisions, making those reevaluations less efficient (*SI Appendix*, Fig. S12). Taken together, these suggest that foraging reevaluations and self-control capabilities were differentially disrupted independent from initial commitment valuations.

Last, all mice were killed, and slices were prepared for the ex vivo IO assay measuring the strength of synaptic transmission of the IL–NAcSh circuit. We calculated IO slopes and correlated them against offer-zone and wait-zone thresholds over the final 5 d of testing (Fig. 3*A*, gold time point). We found a significant correlation between synaptic strength of the IL–NAcSh circuit and wait-zone thresholds but not offer-zone thresholds (correcting for multiple comparisons; offer zone: Pearson $r = -0.225$, $P = 0.23$; wait zone: Pearson $r = -0.509$, $P < 0.01$) (Fig. 3*D*). To ensure that the 10-Hz group (whose behavior was augmented by our plasticity intervention) was not driving this effect, we reran correlations excluding this group and found that the correlation between wait-zone thresholds and synaptic strength of the IL–NAcSh circuit still held (offer zone: $r = -0.325$, $P = 0.16$; wait zone: $r = -0.499$, $P < 0.05$).

Discussion

Based on recent advances in neuroeconomics, distinct valuation algorithms are thought to be processed in separable neural circuits (17). Thus, it is becoming less clear that reward value is calculated in a common currency through a common neural pathway in the brain (18, 20). The IL–NAcSh circuit has been suggested to play a modulatory role regulating motivated behaviors distinct from primary reward valuation processes; however, separating

the two is difficult using traditional behavioral tasks (10). Furthermore, circuit interrogation approaches that rely on nonphysiological manipulations during on-going behavior obscure interpretations of the functional consequences of synaptic remodeling on endogenous information processing. In this study, we directly tested the role of the strength of synaptic transmission in the IL–NAcSh circuit in a neuroeconomic task capable of behaviorally separating fundamentally distinct aspects of decision-making information processing.

We found that induction of LTD of glutamatergic IL projections to the NAcSh produced lasting changes in wait-zone valuation processes but not in offer-zone valuation processes, even though they were measured within the same trial. Behaviorally dissociable changes in distinct economic valuation algorithms occurred without affecting other potentially confounding factors, such as disruptions in locomotor capabilities, knowledge of the rules of the task, or ability to remember locations and spatial relationships, none of which changed under the manipulation (*SI Appendix*, Figs. S8 and S9). Dissociating multiple valuation processes from these other behavioral processes is difficult using standard tasks (e.g., operant place preference, lever pressing, nose poking, or Barnes or Morris mazes) that were not designed for valuation-process separations. These standard tasks generally embed instances of distinct valuation algorithms that are overlapping or are masked by producing indistinguishable consequences.

The separate offer and wait zones used in the Restaurant Row task allowed us to dissociate principal valuations and reevaluative processes by separating them into two stages of reward-seeking decision-making on every trial. What makes this task economic in nature is that it forces subjects to choose between competing options of varying preferences (flavors) in conflict with varying costs (delays) while hungry and on a limited time budget. In this paradigm, mice were tasked with making decisions based on cost information randomly provided at the start of each trial (i.e., at each entry into a restaurant offer zone). Because mice treat these different tones differently in each restaurant, we know that they have the ability to discriminate cost information and that different values can be ascribed to the tones based on subject preferences that are updated and acted upon differently on every trial (*SI Appendix*, Fig. S9). Each trial elicited different sets of discrete actions measurable separately in the offer zone and the wait zone. This separation gave us access to different behavioral computations rooted in fundamentally distinct economic valuations.

In the offer zone, mice displayed behavioral hallmarks of deliberative processes when choosing between competing options before making any investment (*SI Appendix*, Fig. S7) (36–38). To invest in the decision, mice had to enter the wait zone. In the wait zone, mice either waited out the cued delay or abandoned an on-going investment. Behavioral and economic models suggest that these two processes in the offer zone and wait zone arise from distinct economic processes of intertemporal choice—deliberative vs. foraging valuation algorithms, respectively—that are thought to be rooted in separable neural circuits (18, 20, 29, 39–49); however, causal evidence that these processes arise from separable neural circuits has been lacking. Our data definitively show that the strength of synaptic transmission of the IL–NAcSh glutamatergic circuit is causally involved in reevaluations within the wait zone but not in primary valuations in the offer zone.

Studies of extinction and reinstatement behavior in both reward seeking and fear learning support the idea that the IL is crucial, not for expression of principal (i.e., initial) reward or fear valuations but rather for the acquisition of subsequent extinction learning and the maintenance of extinction memory (10, 50–53). Inactivation of the IL has no immediate effect on initial reward-seeking behaviors or fear responses (54–58). However, inactivation of the IL impairs key learning processes so that subjects are unable update regulatory valuations to extinguish these behaviors (54–58). Furthermore, inactivation of IL after extinction learning takes place can provoke spontaneous reinstatement behaviors by lesioning regulatory processes (22). Disconnection experiments and more recent circuit-specific chemogenetic and optogenetic studies have identified the IL projections to the NAcSh or amygdala as more refined pathways implicated in these top-down regulatory processes (for reward and fear, respectively) (23, 24, 59–62). Focusing on reward-related behaviors, inhibition of glutamatergic IL–NAcSh projections time-locked to reinstatement-provoking cues enhanced reinstatement, while excitation of these projections during cue presentation reduced reinstatement (23). In IL, extinction learning processes were protein synthesis-dependent and sensitive to manipulations of neurotrophic factors, cell-adhesion molecules, and synaptic plasticity (13–16, 25, 63–66). Although with certain differences, the regulatory role of the IL is generally in register across both reward-seeking and fear-learning tasks (26). Nonetheless, several studies have emphasized key circuit differences in both fear- and reward-related processes. Furthermore, there are reports suggesting that the neural circuits that are engaged when seeking food to emerge from and relieve a food-deprived hunger state may be different from the circuits engaged when seeking food when sated in either surplus or luxury (67–69). The Restaurant Row task captures special economic conflicts in food-deprived states—a critical economic contingency of the task shared across days—between wanting highly desired rewards vs. knowing to resist costly offers and forage elsewhere.

Studies of behavioral extinction support a useful model of how the IL serves a regulatory role modulating valuation processes, a role in which new overriding processes are learned rather than one in which old valuation learning is removed or forgotten (70, 71). However, it remains to be determined how principal valuations (e.g., originally learned reward seeking) and regulatory processes (e.g., secondarily learned overriding processes) might coexist. How are principal valuations and regulatory valuations integrated to produce a single behavioral output as measured in the maintenance or reinstatement of extinguished behaviors? How might they be processed independently during on-going decision-making if at odds with each other, regardless of whether the behavioral output is extinguished or reinstated? It would appear that the weight of these separable processes is critical in determining how they compete with each other in parallel. Our data find that, using a neuroeconomic approach, principal valuations can be behaviorally segregated from reevaluative processes characterized as change-of-mind decisions within the same trial. Here, we find that reevaluative processes, but not the principal valuations measured in the same trial, are independently sensitive to off-line changes in the strength of synaptic transmission of the glutamatergic IL–NAcSh circuit. Our data implicate a role of the IL–NAcSh circuit in the top-down control of motivated behavior consistent with previous work; here, however, we find that plasticity-augmenting manipulations on a neuroeconomic task reveal this is a neural process separate from and in parallel with on-going principal valuations.

Our findings also provide proof-of-principal experiments for a technological advance in circuit-specific plasticity assessment at the ensemble level. We demonstrate how an assay can be used to explain individual differences in distinct aspects of behavior using such circuit-strength metrics for between-subject comparisons.

We were able to measure the synaptic strength of the glutamatergic IL–NAcSh circuit at the ensemble-level in optogenetically evoked recordings prepared ex vivo. Measuring the strength of synaptic transmission between neurons is a daunting technical challenge. Approaches have historically resorted to electrophysiological recordings of electrical stimulation-evoked postsynaptic responses to glean a metric of state of synaptic plasticity. That is, the degree of change in postsynaptic responses elicited using the same electrical stimulation tested before and after a plasticity-inducing intervention has often served as a way to assay plasticity itself. Rather than being limited to measuring plasticity

merely as a change in response from baseline, which is generally useful only for within-subject comparisons, strides have made in developing single-measurement assays that can capture the strength of synaptic transmission, enabling studies of experience-dependent forms of plasticity useful for between-subject comparisons. Unfortunately, these assays rely on single-cell–level intracellular recordings generally measured only ex vivo using transient bath application of pharmacological agents (e.g., AMPAR/NMDAR ratio metrics) (35). Evoked field recordings performed at the population ensemble level are readily accessible in vivo but have been limited to short-windowed, within-subject measures of plasticity. Other ensemble measures of plasticity have relied on using oscillatory functional coherence measures, but this requires multisite recordings, does not directly reflect the strength of synaptic transmission, and is feasible only in vivo in an intact whole brain (72).

Here, we developed an approach to this problem using optogenetics. Our method of measuring circuit-specific plasticity in an input-specific manner relies on the selective release of glutamate coupled with measurements of relationships between the degree of presynaptic recruitment and postsynaptic responses while directly activating only afferents without introducing stimulus artifacts. This method provides an assay of the strength of synaptic transmission in a projection-specific circuit that is comparable across animals without relying on a whole-cell patch-clamp approach (35). This demonstrates circuit-specific plasticity between two brain regions measured at the ensemble level that relies on only a single measurement and enables between-subject comparisons. This assay revealed that stronger connections from excitatory IL neurons to the NAcSh measured at the ensemble level were found in individuals with increased capabilities to overturn initial principal valuations. Strength of the IL–NAcSh circuit varied independently of individual differences in principal valuations.

In this study, pathway specificity lies in the identity of the presynaptic neuron. Future studies may be able to take advantage of combinatorial and intersection conditional genetic approaches to restrict opsin expression in afferents onto specific postsynaptic neuron subpopulations. For example, several studies have demonstrated functional differences in subpopulations of NAcSh medium spiny neurons depending on their receptor expression profile (e.g., dopamine D1 vs. D2 receptors) (13, 73, 74). Thus, it is possible that ensemble-level measures as well as augmentations of plasticity of glutamatergic afferents from IL exclusively onto one of these two NAcSh subpopulations may give rise to further circuit specialization. Red-shifted excitatory opsins, for example, could be used to assay the strength of synaptic transmission from a second input (e.g., glutamatergic hippocampal projections) into the NAcSh with subsequent red-light assays. Although demonstrated here ex vivo, future studies will be able to take advantage of this assay and leverage the many cross-sectional and multicircuit tools made available through optogenetic approaches both in vivo and ex vivo using the same methodology. By applying this recording assay with optogenetically evoked local field potentials in vivo, future studies would be able to measure the circuit-specific strength of synaptic transmission in animals longitudinally using repeated assays.

The 10-Hz stimulation protocol we used has been previously shown to induce LTD in the IL–NAcSh circuit (13–15, 34, 35). The proposed mechanism of this protocol is dependent on extrasynaptic metabotropic glutamate receptors that signal downstream endocytosis of postsynaptic AMPARs, unlike the NMDAR-mediated LTD demonstrated with lower-frequency protocols (e.g., 1 Hz) (13–15, 34, 35). The 100-Hz protocol has been shown to induce long-term potentiation (LTP) in other circuits; however, this elicited no change in synaptic strength in our experiment (13–15, 34, 35). Furthermore, the induction of LTP in such studies often relied on patching onto the postsynaptic neuron and holding it at a depolarized potential, making measurements at the field level as well as translation to in vivo delivery difficult. Therefore, we used 100-Hz bursts as a protocol, controlling for light exposure and stimulus timing, in addition to the no-stimulation control group. Furthermore, our repeated-measures cross-over design rules out order effects of stimulation protocols. Induction of heterosynaptic plasticity or retrograde action potentials upon IL terminal stimulation in the NAcSh are potential issues to consider. However, despite this, our synaptic strength assay of the glutamatergic IL–NAcSh circuit was capable of capturing plasticity manipulations delivered in vivo and, importantly, could explain individual behavioral differences in reevaluation processes separate from principal valuations in animals with more vs. less potentiated IL–NAcSh synapses.

These findings have significant implications for how specific aspects of decision-making can be processed in a projection-specific circuit, gated by the strength of synaptic transmission of that circuit. Maladaptive plasticity is often observed in neuropsychiatric disorders characterized by impairments in decision-making and behavioral regulation, including addiction. Thus, such individuals could greatly benefit from neuromodulation therapies that induce long-lasting changes in plasticity. There is a growing interest in applying neuromodulation therapies in clinical settings, including the use of transcranial magnetic or deep brain stimulation. However, little attention is often paid toward appreciating what plasticity changes might be induced by these treatments over time. Given the complex heterogeneous cellular architecture and connectivity of the NAcSh, nonspecific neuromodulation can give rise to unpredictable plasticity changes. Plasticity manipulations in animal models of addiction using simple behavioral tests have yielded conflicting findings, preventing relapse-like behaviors in some cases but provoking them in others. Thus, one becomes wary that interventions intended to provide therapeutic benefit could potentially worsen disease states. Therefore, future translational studies will require careful interventions tailored to computation-specific dysfunctions that can be revealed only by moving beyond simple tests of value in conjunction with gain-altering circuit manipulations. Only then can we begin to understand the functional consequences of either disease-provoked or intervention-induced synaptic remodeling on complex information processing (75).

Materials and Methods

Animals. Thirty C57BL/J6 male mice (13 wk old) were used (*SI Appendix, Supplementary Materials and Methods*). All experiments were approved by the University of Minnesota Institutional Animal Care and Use Committee.

Surgery. AAV8-Syn-Chronos-GFP (University of North Carolina at Chapel Hill Vector Core) was bilaterally injected into the IL. The following week mice were bilaterally implanted with optic fibers in the NAcSh.

Electrophysiology. Extracellular optogenetically evoked field recordings in the NAcSh were performed in acute sagittal slices (250 μM) (*SI Appendix, Supplementary Materials and Methods*).

Behavior. Mice implanted with virus-infected optic fiber in the IL/NAcSh were trained on the Restaurant Row task for 70 consecutive days before undergoing a series of acute optogenetic stimulation protocols delivered outside behavioral testing (*SI Appendix, Supplementary Materials and Methods*)

ACKNOWLEDGMENTS. We thank members of the A.D.R. and M.J.T. laboratories, the MnDRIVE Optogenetics Core of the University of Minnesota, Dr. Patrick Rothwell, Dr. Michael Benneyworth, Dr. Manuel Esguerra, Cody Walters, Brendan Hasz, and Caleb Fink for helpful discussions and technical assistance; Ethan Huffington for assistance with surgeries; and Amber McLaughlin, Colleen Hutchison, Madeline Jones, Frank Valdes, Maya Smith, Peter Nicholson, Delfina Mancebo, and Nolan Trevino for help with mouse testing. This research was supported by National Institute on Drug Abuse Grants R01 DA019666, R01 DA030672, R01 DA052808, and F30 DA043326; National Institute of Mental Health Grants R01 MH080318 and R01 MH112688; National Institute of General Medical Sciences Grants 5T32GM008244-25 and 5T32GM008471-22; University of Minnesota MnDRIVE Neuromodulation Research Fellowship; and the Breyer-Longden Family Research Foundation.

1. Robinson TE, Berridge KC (2003) Addiction. *Annu Rev Psychol* 54:25–53.
2. Morales M, Margolis EB (2017) Ventral tegmental area: Cellular heterogeneity, connectivity and behaviour. *Nat Rev Neurosci* 18:73–85.
3. Lüscher C, Malenka RC (2011) Drug-evoked synaptic plasticity in addiction: From molecular changes to circuit remodeling. *Neuron* 69:650–663.
4. Redish AD, Mizumori SJ (2015) Memory and decision making. *Neurobiol Learn Mem* 117:1–3.
5. Hyman SE (2005) Addiction: A disease of learning and memory. *Am J Psychiatry* 162: 1414–1422.
6. Hyman SE, Malenka RC (2001) Addiction and the brain: The neurobiology of compulsion and its persistence. *Nat Rev Neurosci* 2:695–703.
7. van der Meer MA, Johnson A, Schmitzer-Torbert NC, Redish AD (2010) Triple dissociation of information processing in dorsal striatum, ventral striatum, and hippocampus on a learned spatial decision task. *Neuron* 67:25–32.
8. Stott JJ, Redish AD (2014) A functional difference in information processing between orbitofrontal cortex and ventral striatum during decision-making behaviour. *Philos Trans R Soc Lond B Biol Sci* 369:20130472.
9. German PW, Fields HL (2007) Rat nucleus accumbens neurons persistently encode locations associated with morphine reward. *J Neurophysiol* 97:2094–2106.
10. Barker JM, Taylor JR, Chandler LJ (2014) A unifying model of the role of the infralimbic cortex in extinction and habits. *Learn Mem* 21:441–448.
11. Camchong J, et al. (2014) Changes in resting functional connectivity during abstinence in stimulant use disorder: A preliminary comparison of relapsers and abstainers. *Drug Alcohol Depend* 139:145–151.
12. Hearing M, Graziane N, Dong Y, Thomas MJ (2018) Opioid and psychostimulant plasticity: Targeting overlap in nucleus accumbens glutamate signaling. *Trends Pharmacol Sci* 39:276–294.
13. Hearing MC, et al. (2016) Reversal of morphine-induced cell-type-specific synaptic plasticity in the nucleus accumbens shell blocks reinstatement. *Proc Natl Acad Sci USA* 113:757–762.
14. Pascoli V, et al. (2014) Contrasting forms of cocaine-evoked plasticity control components of relapse. *Nature* 509:459–464.
15. Pascoli V, Turiault M, Lüscher C (2011) Reversal of cocaine-evoked synaptic potentiation resets drug-induced adaptive behaviour. *Nature* 481:71–75.
16. Ma Y-Y, et al. (2014) Bidirectional modulation of incubation of cocaine craving by silent synapse-based remodeling of prefrontal cortex to accumbens projections. *Neuron* 83:1453–1467.
17. Redish AD (2013) *The Mind within the Brain: How We Make Decisions and How those Decisions Go Wrong* (Oxford Univ Press, New York).
18. Redish AD, Jensen S, Johnson A (2008) A unified framework for addiction: Vulnerabilities in the decision process. *Behav Brain Sci* 31:415–437, discussion 437–487.
19. Walters CJ, Redish AD (2017) A case study in computational psychiatry: Addiction as failure modes of the decision-making system. *Computational Psychiatry: Mathematical Modeling of Mental Illness*, eds Anticevic A, Murray J (Academic Press, Cambridge, MA), pp 199–217.
20. Rangel A, Camerer C, Montague PR (2008) A framework for studying the neurobiology of value-based decision making. *Nat Rev Neurosci* 9:545–556.
21. Bickel WK, Jarmolowicz DP, Mueller ET, Gatchalian KM, McClure SM (2012) Are executive function and impulsivity antipodes? A conceptual reconstruction with special reference to addiction. *Psychopharmacology (Berl)* 221:361–387.
22. Peters J, LaLumiere RT, Kalivas PW (2008) Infralimbic prefrontal cortex is responsible for inhibiting cocaine seeking in extinguished rats. *J Neurosci* 28:6046–6053.
23. Gutman AL, et al. (2017) Extinction of cocaine seeking requires a window of infralimbic pyramidal neuron activity after unreinforced lever presses. *J Neurosci* 37:6075–6086.
24. Augur IF, Wyckoff AR, Aston-Jones G, Kalivas PW, Peters J (2016) Chemogenetic activation of an extinction neural circuit reduces cue-induced reinstatement of cocaine seeking. *J Neurosci* 36:10174–10180.
25. Gass JT, Chandler LJ (2013) The plasticity of extinction: Contribution of the prefrontal cortex in treating addiction through inhibitory learning. *Front Psychiatry* 4:46.
26. Peters J, Kalivas PW, Quirk GJ (2009) Extinction circuits for fear and addiction overlap in prefrontal cortex. *Learn Mem* 16:279–288.
27. Creed M, Pascoli VJ, Lüscher C (2015) Addiction therapy. Refining deep brain stimulation to emulate optogenetic treatment of synaptic pathology. *Science* 347:659–664.
28. Kalenscher T, van Wingerden M (2011) Why we should use animals to study economic decision making–A perspective. *Front Neurosci* 5:82.
29. Sweis B, Thomas M, Redish A (2018) Mice learn to avoid regret. *PLoS Biol*, in press.
30. Steiner AP, Redish AD (2014) Behavioral and neurophysiological correlates of regret in rat decision-making on a neuroeconomic task. *Nat Neurosci* 17:995–1002.
31. Klapoetke NC, et al. (2014) Independent optical excitation of distinct neural populations. *Nat Methods* 11:338–346.
32. Britt JP, et al. (2012) Synaptic and behavioral profile of multiple glutamatergic inputs to the nucleus accumbens. *Neuron* 76:790–803.
33. Brog JS, Salyapongse A, Deutch AY, Zahm DS (1993) The patterns of afferent innervation of the core and shell in the "accumbens" part of the rat ventral striatum: Immunohistochemical detection of retrogradely transported fluoro-gold. *J Comp Neurol* 338:255–278.
34. Thomas MJ, Malenka RC, Bonci A (2000) Modulation of long-term depression by dopamine in the mesolimbic system. *J Neurosci* 20:5581–5586.
35. Thomas MJ, Beurrier C, Bonci A, Malenka RC (2001) Long-term depression in the nucleus accumbens: A neural correlate of behavioral sensitization to cocaine. *Nat Neurosci* 4:1217–1223.
36. Redish AD (2016) Vicarious trial and error. *Nat Rev Neurosci* 17:147–159.
37. Muenzinger KF (1956) On the origin and early use of the term vicarious trial and error (VTE). *Psychol Bull* 53:493–494.
38. Tolman EC (1939) Prediction of vicarious trial and error by means of the schematic sowbug. *Psychol Rev* 46:318–336.
39. Hare TA, Camerer CF, Rangel A (2009) Self-control in decision-making involves modulation of the vmPFC valuation system. *Science* 324:646–648.
40. McClure SM, Laibson DI, Loewenstein G, Cohen JD (2004) Separate neural systems value immediate and delayed monetary rewards. *Science* 306:503–507.
41. Stephens DW, Krebs JR (1989) *Foraging Theory* (Princeton Univ Press, Princeton).
42. Carter EC, Redish AD (2016) Rats value time differently on equivalent foraging and delay-discounting tasks. *J Exp Psychol Gen* 145:1093–1101.
43. Wikenheiser A, Stephens D, Redish AD (2013) Subjective costs drive overly patient foraging strategies in rats on an intertemporal foraging task. *Proc Natl Acad Sci USA* 110:8308–8313.
44. Stephens DW, Kerr B, Fernández-Juricic E (2004) Impulsiveness without discounting: The ecological rationality hypothesis. *Proc Biol Sci* 271:2459–2465.
45. Kolling N, Akam T (2017) (Reinforcement?) Learning to forage optimally. *Curr Opin Neurobiol* 46:162–169.
46. Ainslie G (1975) Specious reward: A behavioral theory of impulsiveness and impulse control. *Psychol Bull* 82:463–496.
47. Redish AD, Schultheiss NW, Carter EC (2016) The computational complexity of valuation and motivational forces in decision-making processes. *Curr Top Behav Neurosci* 27:313–333.
48. Charnov EL (1976) Optimal foraging, the marginal value theorem. *Theor Popul Biol* 9: 129–136.
49. Papale AE, Stott JJ, Powell NJ, Regier PS, Redish AD (2012) Interactions between deliberation and delay-discounting in rats. *Cogn Affect Behav Neurosci* 12:513–526.
50. Milad MR, Quirk GJ (2002) Neurons in medial prefrontal cortex signal memory for fear extinction. *Nature* 420:70–74.
51. Zeeb FD, Baarendse PJ, Vanderschuren LJ, Winstanley CA (2015) Inactivation of the prelimbic or infralimbic cortex impairs decision-making in the rat gambling task. *Psychopharmacology (Berl)* 232:4481–4491.
52. Chudasama Y, Robbins TW (2003) Dissociable contributions of the orbitofrontal and infralimbic cortex to pavlovian autoshaping and discrimination reversal learning: Further evidence for the functional heterogeneity of the rodent frontal cortex. *J Neurosci* 23:8771–8780.
53. Sierra-Mercado D, Padilla-Coreano N, Quirk GJ (2011) Dissociable roles of prelimbic and infralimbic cortices, ventral hippocampus, and basolateral amygdala in the expression and extinction of conditioned fear. *Neuropsychopharmacology* 36:529–538.
54. LaLumiere RT, Niehoff KE, Kalivas PW (2010) The infralimbic cortex regulates the consolidation of extinction after cocaine self-administration. *Learn Mem* 17:168–175.
55. Keistler C, Barker JM, Taylor JR (2015) Infralimbic prefrontal cortex interacts with nucleus accumbens shell to unmask expression of outcome-selective Pavlovian-to-instrumental transfer. *Learn Mem* 22:509–513.
56. Lebrón K, Milad MR, Quirk GJ (2004) Delayed recall of fear extinction in rats with lesions of ventral medial prefrontal cortex. *Learn Mem* 11:544–548.
57. Quirk GJ, Russo GK, Barron JL, Lebron K (2000) The role of ventromedial prefrontal cortex in the recovery of extinguished fear. *J Neurosci* 20:6225–6231.
58. Laurent V, Westbrook RF (2009) Inactivation of the infralimbic but not the prelimbic cortex impairs consolidation and retrieval of fear extinction. *Learn Mem* 16:520–529.
59. Do-Monte FH, Manzano-Nieves G, Quiñones-Laracuente K, Ramos-Medina L, Quirk GJ (2015) Revisiting the role of infralimbic cortex in fear extinction with optogenetics. *J Neurosci* 35:3607–3615.
60. Bossert JM, et al. (2012) Role of projections from ventral medial prefrontal cortex to nucleus accumbens shell in context-induced reinstatement of heroin seeking. *J Neurosci* 32:4982–4991.
61. Kim CK, et al. (2017) Molecular and circuit-dynamical identification of top-down neural mechanisms for restraint of reward seeking. *Cell* 170:1013–1027.e14.
62. LaLumiere RT, Smith KC, Kalivas PW (2012) Neural circuit competition in cocaine-seeking: Roles of the infralimbic cortex and nucleus accumbens shell. *Eur J Neurosci* 35:614–622.
63. Barker JM, Torregrossa MM, Taylor JR (2012) Low prefrontal PSA-NCAM confers risk for alcoholism-related behavior. *Nat Neurosci* 15:1356–1358.
64. Peters J, Dieppa-Perea LM, Melendez LM, Quirk GJ (2010) Induction of fear extinction with hippocampal-infralimbic BDNF. *Science* 328:1288–1290.
65. Barker JM, Taylor JR, De Vries TJ, Peters J (2015) Brain-derived neurotrophic factor and addiction: Pathological versus therapeutic effects on drug seeking. *Brain Res* 1628:68–81.
66. Santini E, Ge H, Ren K, Peña de Ortiz S, Quirk GJ (2004) Consolidation of fear extinction requires protein synthesis in the medial prefrontal cortex. *J Neurosci* 24:5704–5710.
67. Calhoon G, et al. (2018) Acute food deprivation rapidly modifies valence-coding microcircuits in the amygdala. bioRxiv:10.1101/285189.
68. Beyeler A, et al. (2016) Divergent routing of positive and negative information from the amygdala during memory retrieval. *Neuron* 90:348–361.
69. Namburi P, et al. (2015) A circuit mechanism for differentiating positive and negative associations. *Nature* 520:675–678.
70. Bouton ME (2004) Context and behavioral processes in extinction. *Learn Mem* 11:485–494.
71. Rescorla RA (2001) Retraining of extinguished Pavlovian stimuli. *J Exp Psychol Anim Behav Process* 27:115–124.
72. O'Neill P-K, Gordon JA, Sigurdsson T (2013) Theta oscillations in the medial prefrontal cortex are modulated by spatial working memory and synchronize with the hippocampus through its ventral subregion. *J Neurosci* 33:14211–14224.
73. Calipari ES, et al. (2016) In vivo imaging identifies temporal signature of D1 and D2 medium spiny neurons in cocaine reward. *Proc Natl Acad Sci USA* 113:2726–2731.
74. Keeler JF, Pretsell DO, Robbins TW (2014) Functional implications of dopamine D1 vs. D2 receptors: A 'prepare and select' model of the striatal direct vs. indirect pathways. *Neuroscience* 282:156–175.
75. Redish AD, Gordon JA (2016) *Computational Psychiatry: New Perspectives on Mental Illness* (MIT Press, Cambridge, MA).